Engineering 57 (2026) 126–137

Contents lists available at ScienceDirect

Engineering

journal homepage: www.elsevier.com/locate/eng

Research
Glycomedicine—Article

The Serum-Derived Extracellular Vesicle N-Glycome as a New Biosignature for Childhood Epilepsy

Yuanyuan Liu [a,#], Yanbin Guo [a,#], Changzhen Li [b], Zhiwen Huang [a], Xiang Liu [b], Han Xie [a], Wenhui Wang [a], Lili Guan [c], Bi-Feng Liu [a], Si Liu [d,*], Guoping Wang [a,*], Xin Liu [a,*]

[a] The Key Laboratory of Molecular Biophysics of MOE and Hubei Bioinformatics & Molecular Imaging Key Laboratory, Department of Biomedical Engineering, College of Life Science and Technology, Huazhong University of Science and Technology, Wuhan 430074, China
[b] Department of Laboratory Medicine, Wuhan Children's Hospital, Tongji Medical College, Huazhong University of Science and Technology, Wuhan 430016, China
[c] Tongji Hospital of Tongji Medical College, Huazhong University of Science and Technology, Wuhan 430030, China
[d] Department of Epidemiology and Health Statistics, School of Public Health, Fujian Medical University, Fuzhou 350122, China

ARTICLE INFO

Article history:
Received 14 April 2025
Revised 7 November 2025
Accepted 5 December 2025
Available online 19 December 2025

Keywords:
Epilepsy
Extracellular vesicles
N-glycans
Machine learning
Diagnosis

ABSTRACT

Childhood epilepsy poses a serious threat to patients' growth, development, and life safety, creating an urgent need for precise, non-invasive, and longitudinally monitorable biomarkers. Previous studies have confirmed that extracellular vesicles (EVs) with abnormal N-glycosylation modifications regulate various neurological disorders, where characteristic *N*-glycans serve as potential diagnostic markers. In this study, we systematically compared the properties of EVs isolated via three different methods. The results demonstrated that an exosome purification filter column (EPF) combined with ultrafiltration emerged as the optimal approach for isolating EVs from large-scale clinical samples. Subsequent matrix-assisted laser desorption ionization time-of-flight mass spectrometry (MALDI-TOF-MS)-based glycomic profiling of EVs and serum revealed distinct *N*-glycan signatures. Utilizing a novel two-step machine learning model, we identified 47 characteristic *N*-glycans in EVs as biomarkers for epilepsy diagnosis and classification. These biomarkers effectively distinguished between normal, focal, and generalized epilepsy subtypes while also exhibiting superior diagnostic performance compared to serum *N*-glycan profiles. Furthermore, we constructed a correlation network map of glycans, which highlighted dynamic alterations in the expression patterns of EV glycans during epileptogenesis. Taken together, the *N*-glycans of EVs exhibit promising potential as biomarkers for epilepsy detection, offering new insights into non-invasive diagnosis and disease monitoring.

© 2025 THE AUTHORS. Published by Elsevier LTD on behalf of Chinese Academy of Engineering and Higher Education Press Limited Company. This is an open access article under the CC BY license (http://creativecommons.org/licenses/by/4.0/).

1. Introduction

Epilepsy is a chronic neurological disorder characterized by recurrent seizures resulting from abnormal neuronal hyperexcitability. The disease presents as a bimodal age distribution with peaks at ages 5–9 and around 80 years old [1]. Patients face a threefold higher risk of premature mortality, and the condition affects over 70 million people, with 60% of cases beginning in childhood [2]. Current diagnostic methods—clinical history, electroencephalogram (EEG), and neuroimaging—have significant limitations: clinical history is subjective, EEG lacks sensitivity in detecting focal seizures, and neuroimaging often produces nonspecific readouts [3]. These challenges highlight the need for improved monitoring techniques and the identification of precise biomarkers for early detection [3–5].

Liquid biopsies play an important function in early detection of childhood epilepsy, as well as contributing to understanding etiology, and for therapeutic monitoring. Serum is commonly used and easily accessible for detection purposes; however, its complexity often obscures disease signals [6]. Extracellular vesicles (EVs) are defined as cell-released, lipid-bilayer-delimited particles that cannot replicate on their own and are ubiquitous in various biofluids [7]. As EVs play important roles in physiological and pathological

* Corresponding authors.
E-mail addresses: siliu@fjmu.edu.cn (S. Liu), wangguoping@hust.edu.cn (G. Wang), xliu@mail.hust.edu.cn (X. Liu).
# These authors contributed equally to this work.

https://doi.org/10.1016/j.eng.2025.12.009
2095-8099/© 2025 THE AUTHORS. Published by Elsevier LTD on behalf of Chinese Academy of Engineering and Higher Education Press Limited Company.
This is an open access article under the CC BY license (http://creativecommons.org/licenses/by/4.0/).

pathways, they represent a promising biomarker candidate for liquid biopsy applications [8]. In recent years, development of novel exosome-based diagnostic technologies has increased, driven by advances in methodologies such as microfluidics [9], electric field enhancement [10,11], and nanomaterials [12]. Notably, efficient EV enrichment is critical for molecular analysis and diagnostics. The separation process significantly influences the quality and molecular characteristics of EVs; however, standardization of isolation methods is limited and further optimization for clinical biological samples is also warranted [13]. Current techniques, including ultracentrifugation (UC), size-exclusion chromatography (SEC), and immunoaffinity capture, often co-isolate impurities, compromising purity and yield [14,15]. To address these limitations, the integration of complementary methods and systematic workflow optimization is crucial for obtaining high-purity, high-yield EV preparations and for ensuring clinical reliability.

Glycosylation patterns of serum glycoproteins correlate with inflammatory responses and disease progression, underscoring the potential of *N*-glycans in disease stratification [16]. Despite growing interest in EVs, studies on their glycosylation remain limited. EVs transport diverse cargoes and exhibit differential glycosylation patterns on protein and lipid components, influencing biogenesis, intercellular communication, and disease progression due to structural diversity and synthetic complexity of EV surface glycans [17–19]. Thus, EV glycans show promise as biomarkers in cancers [20,21] and neurological disorders [22,23]. Although research on glycosylation profiles for epilepsy is not extensive, growing evidence suggests that abnormal N-glycosylation of membrane proteins, including ion channels and receptors, may enhance neuronal excitability, leading to seizures [24–28]. Furthermore, seizures increase blood–brain barrier (BBB) permeability and the natural ability of EVs to freely cross the BBB, further enabling EVs entry into systemic circulation [29]. Emerging evidence indicates that EVs released by brain cells can be detected in peripheral blood [30,31], and their glycans may offer greater diagnostic value than serum glycans. Analyzing EV glycans in childhood epilepsy would enhance the understanding of EV biology and advance translational research towards the development of tools for the diagnosis and treatment of epilepsy. However, current understanding of glycosylation pathways is limited to *in vitro* studies, with *in vivo* validation hindered by complex and technological constraints [32]. Thus, understanding glycosylation at the molecular level could clarify glycan regulation in epilepsy and explore pathogenic mechanisms in childhood epilepsy.

Artificial intelligence (AI) has revolutionized biomarker identification, enabling rapid image interpretation, cancer biomarker discovery, and early diagnosis [33]. It has been widely applied in cancer screening [21,34]. Traditional statistical approaches in glycomics research, such as the Wilcoxon–Mann–Whitney test [35] and partial least squares discriminant analysis [36], focus on isolated glycan features, while machine learning is highly effective in analyzing complex glycan–disease interactions, thus improving the identification of diagnostics and biomarkers. Collectively, AI and machine learning approaches show promise for exploring EV N-glycosylation in childhood epilepsy, identifying glycan biomarkers, and developing predictive models for stratified management of epilepsy.

In this study, we first assessed the impact of three advanced EV separation methods—differential UC, reagent precipitation (REG), and a combined exosome purification filter column/ultrafiltration approach (EPF/UF, hereafter referred to as EPF)—on EV glycosylation. The EPF was selected for glycomic analysis of EVs in epilepsy. High-throughput matrix-assisted laser desorption ionization time-of-flight mass spectrometry (MALDI-TOF-MS) was applied to analyze serum- and EV-derived N-glycome profiles in healthy controls and childhood epilepsy cohorts stratified by seizure type (focal/-generalized). In an attempt to decode glycomic signatures, a two-step machine learning framework identified potential N-glycome biomarkers and a glycan-based diagnostic model for epilepsy was developed. The model demonstrated robust diagnostic performance, and comparative analysis between the epilepsy cohort and controls emphasized the significance of EV-derived *N*-glycans in epileptogenesis. A glycan interaction network mapped dynamic changes in EV glycans, establishing a novel link between childhood epilepsy and aberrant EV glycosylation, offering new insights into the pathophysiology of epilepsy.

2. Materials and methods

2.1. Serum preparation

All serum samples were collected according to standard procedures and stored in the Wuhan Children's Hospital, China. Whole blood samples were collected and briefly held at room temperature in ethylenediaminetetraacetic acid (EDTA)-coated tubes for less than 30 min. Prior to any processing, a visual inspection was performed to confirm the absence of hemolysis. Subsequently, the blood was centrifuged at 5300 r·min^{-1} for 15 min at room temperature to obtain a cell pellet, and the resulting supernatant was further centrifuged at 9700 r·min^{-1} for 30 min to remove cellular debris and larger vesicles. Serum samples were prepared immediately prior to their application in downstream procedures. For the purpose of methodological comparison, 3 mL of fresh serum obtained from a single donor was evenly distributed into three identical aliquots, with each aliquot being processed using a distinct extraction method. Utilizing samples from the same donor under uniform pretreatment conditions serves to minimize inter-individual variability throughout the experimental process.

2.2. EV isolation

To minimize potential impacts of freezing on sample integrity, EV isolation was conducted immediately after sample acquisition. Three distinct EV isolation techniques were compared in this study: UC, EPF, and an exosome isolation reagent (REG).

(1) The EVs isolated by UC: EVs were isolated by differential centrifugation, which is the most commonly used method. Serum samples underwent sequential centrifugation steps at 4 °C: first at 1600 r·min^{-1} for 10 min, followed by 4300 r·min^{-1} for an additional 10 min, and finally at 9700 r·min^{-1} for 30 min. The supernatant was subsequently passed through a 0.22 μm pore-size filter. Then, the processed serum was subjected to ultracentrifugation at 40 000 r·min^{-1} for 70 min in a polymer tube using a rocking rotor (Type 70Ti; Beckman Coulter, USA) and maintained at 4 °C. The above precipitates were washed using phosphate-buffered saline (PBS) and then centrifuged at 4 °C and 40 000 r·min^{-1} for 70 min. The precipitate of EVs was resuspended in 100 μL of PBS.

(2) The EVs isolated by EPF: EPF was conducted according to the manufacturer's instructions. Briefly, pretreatment of samples: Serum was first centrifuged at 9700 r·min^{-1} for 10 min at 4 °C. The resulting supernatant was then aliquoted into 500 μL aliquots. If the sample volume was insufficient, it was adjusted to 500 μL with PBS. Removal of heterogeneous proteins: 400 μL of pre-chilled protein denaturing buffer (Exosome Extraction & Purification kit; Duolaimi Biotechnology, China) was added to 500 μL of serum sample. The centrifuge tube was immediately sealed tightly and mixed thoroughly for 30 s (followed by prompt centrifugation). The mixture was then subjected to centrifugation at 9700 r·min^{-1} for 20 min at 4 °C to pellet contaminants, following which the clarified supernatant was collected and transferred into a 1.5 mL centrifuge tube. Precipitate of EVs: To the supernatant

obtained after protein precipitation, 120 μL of exosome precipitation reagent (Exosome Extraction & Purification kit; Duolaimi Biotechnology) was added and thoroughly mixed by vortexing for 2 min. The mixture was then incubated at room temperature for 5 min. Subsequently, the tube was centrifuged at 9700 r·min^{-1} and 4 °C for 15 min, followed by careful removal of the supernatant. The pellet was subjected to a second centrifugation under the same conditions (9700 r·min^{-1}, 4 °C) for 2 min, after which the residual supernatant was completely aspirated. Finally, the 1.5 mL tube containing the pellet was left uncapped at room temperature for 10 min to air-dry. Resuspension and recovery of EVs: 200 μL of PBS was added to the precipitate for repeated aspiration and thorough dissolution. Then centrifugation at 4 °C and 9700 r·min^{-1} for 5 min was performed and the supernatant was collected. Purification of EVs: The crude exosome pellet was transferred into the upper chamber of the exosome purification filter column and centrifuged at 4 °C and 5300 r·min^{-1} for 10 min. The fluid from the lower chamber of the EPF column was collected and subjected to two cycles of ultrafiltration (100 kDa), with the resulting filtrate collected as EVs.

(3) The EVs isolated by REG: REG was performed according to the manufacturer's instructions. Briefly, 1/3 volume of RiboTM exosome isolation reagent (for plasma or serum) was added to the resuspended sample and the mixture was inverted until completely mixed. The mixture was incubated at 4 °C for 30 min and then centrifuged at 12 000 r·min^{-1} for 2 min under the same temperature conditions. The supernatant was carefully pipetted off and the exosomes were recovered in the precipitate. Each EV protein concentration was determined using a bicinchoninic acid (BCA) protein assay kit (Beyotime Biotechnology, China).

2.3. Transmission electron microscopy (TEM)

For TEM imaging, freshly isolated EVs were fixed in 4% paraformaldehyde for 30 min. Approximately 5 μL of the suspension was applied to copper grids, allowed to settle for 30 min, and gently blotted to dry. Negative staining was carried out using 5 μL of 1% uranyl acetate for 30 s, followed by removal of excess stain with filter paper. Grids were fully air-dried before observation.

2.4. Nanoparticle tracking analysis (NTA)

The concentration and size distribution of EVs were analyzed by NTA employing a ZetaView system (PMX-120; Particle Metrix, Germany). Prior to sample measurements, the system was calibrated using 100 nm polystyrene standard beads. Data on nanoparticle concentration (expressed as particles·mL^{-1}) were processed and recorded with the integrated NTA software.

2.5. Western blotting

Total protein was extracted from EVs using an exosome-specific lysis buffer, followed by centrifugation at 12000 r·min^{-1} for 10 min at 4 °C. Protein concentration was quantified with a BCA protein assay kit. Proteins were separated by sodium dodecyl sulfate-polyacrylamide gel electrophoresis (SDS-PAGE) and visualized via Coomassie blue staining. Subsequently, proteins were transferred onto polyvinylidene difluoride (PVDF) membranes after electrophoretic separation. Membranes were blocked with 5% skimmed milk for 1 h and then incubated overnight at 4 °C with primary antibodies against CD81, CD63, tumor susceptibility gene 101 coded protein (TSG101), and calnexin. Following three washes with tris buffered saline with Tween 20 (TBST), membranes were incubated with horseradish peroxidase (HRP)-conjugated secondary antibodies for 1 h at room temperature. Finally, protein bands were detected using an enhanced chemiluminescence (ECL) substrate system.

Detailed methods for glycan enrichment and machine learning model construction are provided in Appendix A.

3. Results

3.1. Comparative analysis of three methods for EV isolation

EVs are promising biomarkers for disease diagnostics. To evaluate the efficiency and clinical applicability of methods to isolate EVs, serum-derived EVs were isolated using UC, EPF, and REG, followed by TEM, NTA, Western blotting, and MALDI-TOF-MS (Fig. 1(a)). EVs exhibited a typical cup-shaped structure (60–200 nm), with EPF showing a unimodal peak (Fig. 1(b)). The mean sizes of EPF-EVs were smaller than REG-EVs but slightly larger than UC-EVs (Fig. 1(c)). Notably, the data indicated that EPF-EVs yielded 26-fold (P = 0.033) and 7-fold (P = 0.049) higher outputs compared to UC-EVs and REG-EVs, respectively (Fig. 1(c)).

To estimate the purity of EVs isolated by all three methods, the protein concentrations of EVs were measured. The results indicated that protein concentrations were highest in REG-EVs, followed by UC-EVs and EPF-EVs (Fig. 1(d)). EPF-EVs showed a higher particle/protein ratio relative to REG-EVs and UC-EVs (Fig. 1(e)), indicating enhanced purity. Next, EV samples were verified through Western blotting. As shown in Fig. S1 in Appendix A, EV markers CD63 and CD81 were detected in the isolated EVs. The weak TSG101 signal is likely due to low protein concentration, and the negative control EV marker calnexin was not detected. Taken together, our findings indicated that, using all three methods, EVs were efficiently isolated and thoroughly purified from serum.

Upon evaluating the practical applicability of the three methods, EPF emerged as the optimum technique for isolating EVs for clinical practice.

3.2. Glycomics analysis of serum EVs isolated by EPF, UC, and REG

To confirm the higher feasibility of EPF for isolating EVs, *N*-glycan features of EPF-EVs, UC-EVs, and REG-EVs were compared using MALDI-TOF-MS (Fig. 2(a)). Distinct mass spectra signals indicated varying glycan expression across the three methods (Fig. 2(b)). Following mass confirmation (mass-to-charge ratio (m/z)), baseline correction, and noise filtering of the spectra (signal/noise threshold = 3), 54 *N*-glycans were selected for further analysis (Table S1 in Appendix A). Structures of the selected glycans were confirmed by MALDI-MS/MS (Fig. S2 in Appendix A) and aligned with Ref. [37]. The stability and reproducibility of the analytical process were confirmed through sample quality control (QC) (relative standard deviations (RSDs) < 20%; Table S2 in Appendix A). From the perspective of glycosylation features, radar plots (Fig. 3(a)) showed differences in EV glycan expression, particularly in mannosylation, fucosylation, and sialylation. Furthermore, significant differences in species and distribution were noted among EPF-EVs, UC-EVs, and REG-EVs (Fig. S3(a) in Appendix A).

To determine distinctive features between glycans enriched by the three methods, heterogeneity was rigorously analyzed using post-hoc evaluations of pairwise comparisons. Post-hoc pairwise comparisons quantified glycan expression changes via multiple *P*-value comparisons (Fig. 3(b)), confirming method-specific glycosylation signatures and were consistent with the observed variations in glycan features. Furthermore, sparse partial least squares discriminant analysis (sPLS-DA; Fig. 3(c)) and clustering heatmaps revealed a clear separation of EVs by isolation method (Fig. 3(d), Fig. S3(b) in Appendix A), indicating that methodological variations drive observed differences rather than intrinsic differences. Our

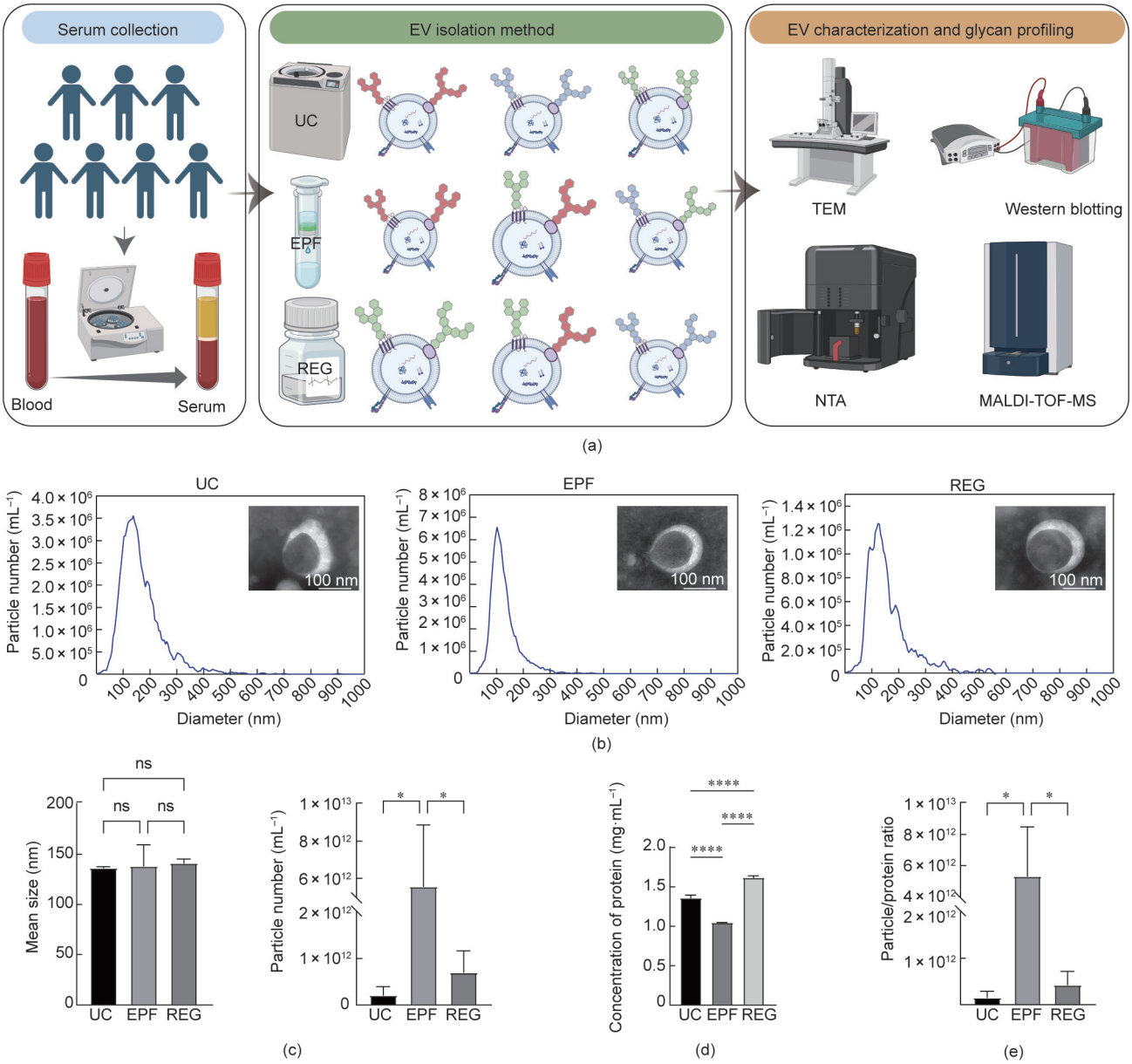

Fig. 1. Characterization of EV separated by distinct methods. (a) Workflow of evaluating EV separated by UC, EPF, and REG. (b) Representative NTA and TEM images of UC-EVs, EPF-EVs, and REG-EVs. (c) Mean size and concentration of UC-EVs, EPF-EVs, and REG-EVs. (d) Protein concentration of the isolated EVs by UC, EPF, and REG was determined by a BCA protein assay kit. (e) The particle/protein ratios of EVs by UC, EPF, and REG. UC-EVs, EPF-EVs, and REG-EVs indicated EVs isolated by UC, EPF, and REG, respectively. $^{*}P < 0.05$; $^{****}P < 0.0001$; ns: no significant difference.

findings suggest that EV glycosylation profiles may be influenced by the isolation technique used.

3.3. Comparative analysis of EV and serum N-glycome profiles

To assess glycan patterns of EVs in clinical sera samples, serum-derived EVs were isolated from healthy donor's sera using EPF and analyzed via glycomic approaches. As EVs are capable of bidirectional transport between the central nervous system and peripheral circulation [31,38], we hypothesized that, in the context of neurological disorders, EV-derived glycans exhibit superior biomarker potential compared to serum glycans. Consequently, we conducted a comprehensive comparative analysis of the glycosylation patterns between serum and EVs. The profiles revealed distinct signals for different mass spectra in serum and EVs, directly indicating the distinctive abundant expression of diverse glycan motifs (Fig. S4 in Appendix A). QC samples confirmed analytical consistency (RSDs < 20%; Table S3 in Appendix A). Further analysis indicated higher neutral and monosialylated glycan levels in EVs, but no significant differences in polysialylated glycans (Fig. S5(a) in Appendix A). Subsequently, detailed differential analysis as represented by volcano plots (Fig. 3(e)) showed a downtrend in the abundance of glycans H5N2, H6N2, and H5N4S1 in EVs, with dominant high mannosylation and sialylation motifs. In contrast, increased glycans included H3N4F1, H4N4F1, H3N5F1, H4N5, H4N4S1, H5N4F1, H4N5F1, and H5N5S2F1, featuring galactosylation, fucosylation, sialylation, and bisection. These findings suggest EVs exhibit specific glycosylation patterns linked to their parent cells' physiological state and type.

We next analyzed differences in glycosylation by comparing glycosylation features in EVs and serum across four categories: high mannose, fucosylation (F), sialylation (S), and galactosylation

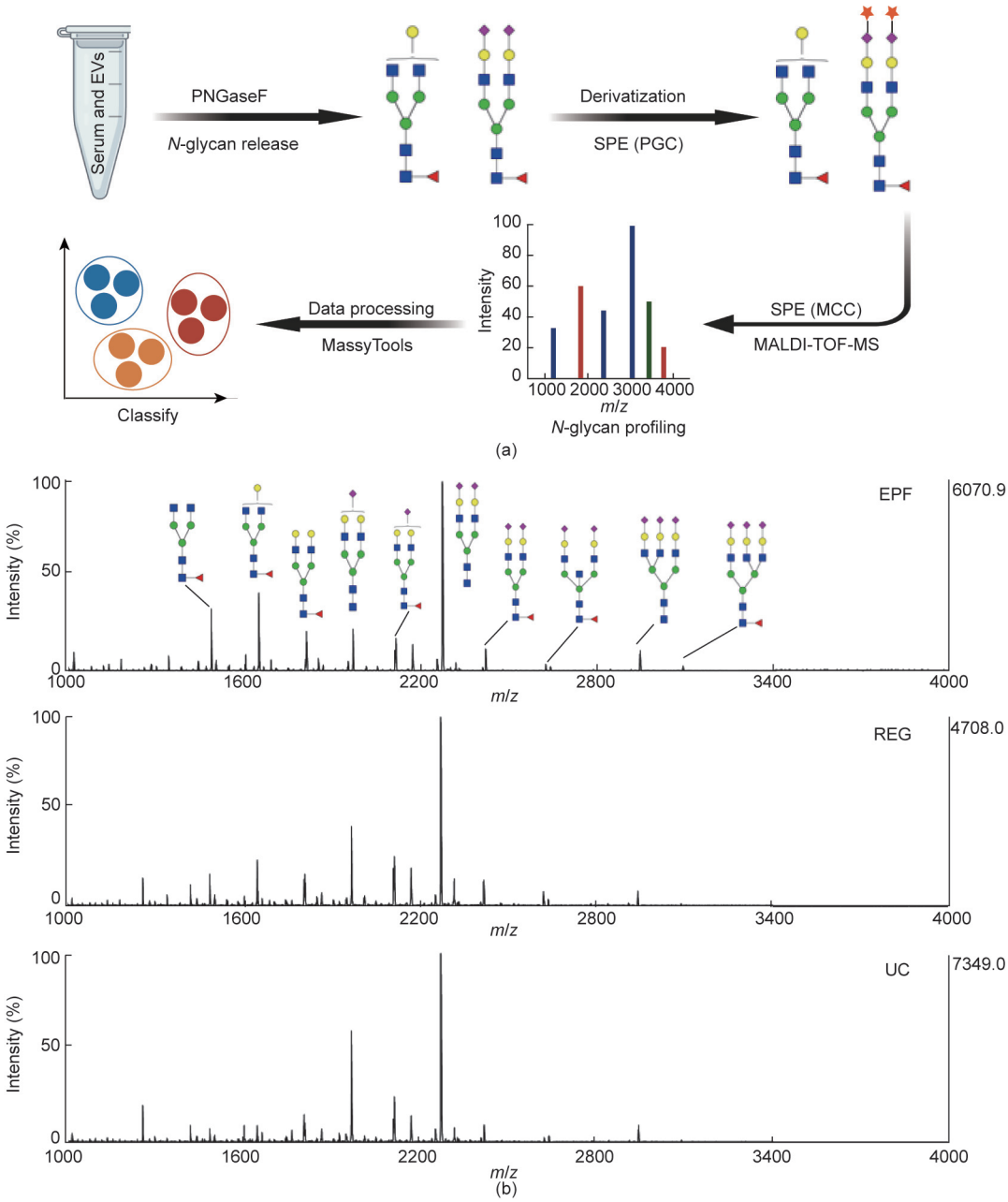

Fig. 2. Workflow of N-glycome and representative MALDI-TOF-MS spectra of the three methods. (a) Workflow of serum and EV *N*-glycans profiling. (b) Representative MALDI-TOF-MS spectra of UC-EVs, EPF-EVs, and REG-EVs *N*-glycan profiles. PNGaseF: peptide *N*-glycosidase F; SPE: solid-phase extraction; PGC: porous graphitic carbon; MCC: cellulose microcrystalline.

(G) (Fig. S5(b) in Appendix A). EVs were enriched in S2 total (31.9%) and F total (17.9%), followed by S1 total (11.5%), F neutral (9.4%), and F sialo (8.1%). In serum, S2 total (45.9%) and S1 total (14.8%) dominated, with F total (10.9%), F sialo (7.6%), and F neutral (3.1%) showing lower expression. Moreover, galactosylation trends were similar in both EVs and serum. Correlation analysis revealed low inter-sample correlations (mostly correlation coefficient (r) < 0.5; Fig. S5(c) in Appendix A) among sample types. Orthogonal partial least squares-discriminant analysis (OPLS-DA) demonstrated clear separation of EVs and serum (Fig. 3(f)), highlighting significant glycosylation pattern variations. These findings emphasize glycosylation complexity and provide insights for further serum and EV glycan analysis. Although lectin arrays are commonly used for EV glycan analysis, expression abundance of individual glycans can be obtained through MALDI-TOF-MS. For large-scale clinical studies, the EPF-MALDI combination is more suitable than lectins. Thus, EPF was used to isolate EVs from epilepsy patients' sera samples.

3.4. N-*glycan analysis of sera and EVs from childhood epilepsy patients*

The clinical applicability of the EPF method was assessed by analyzing glycans in sera and EVs from epilepsy patients using MALDI-TOF-MS (Table S1 and Fig. S6 in Appendix A) and their potential as biomarkers for childhood epilepsy was also explored. Subsequently, OPLS-DA of *N*-glycan data from 218 sera and EV samples was undertaken to comprehensively understand the glycomic landscape and assess meaningful differences in the glycome of childhood epilepsy patients (normal/focal/generalized). Compared to the serum glycome, EV glycan profiles effectively

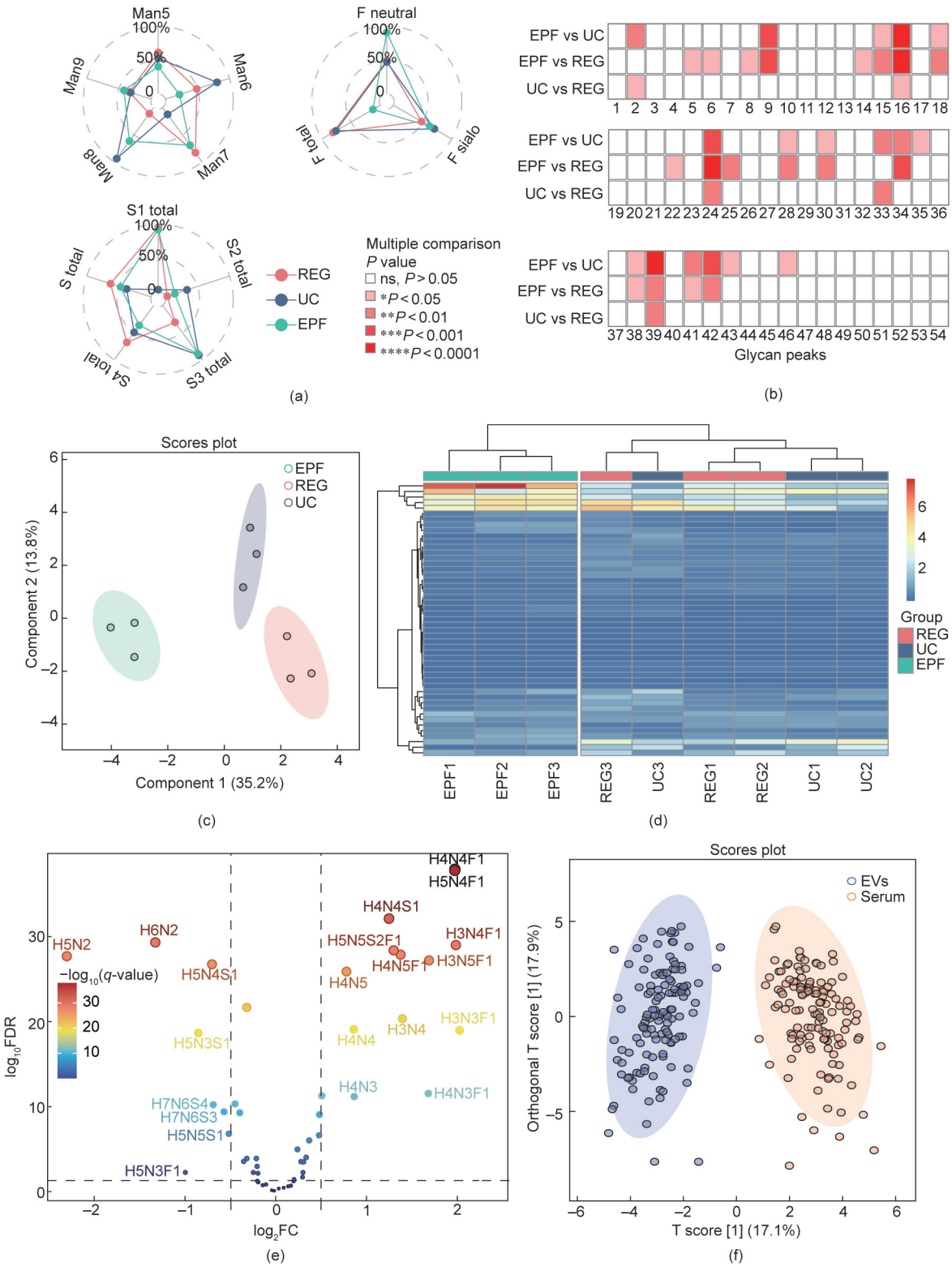

Fig. 3. Evaluation of glycan features of EVs isolated by UC, EPF, and REG from serum of three healthy subjects. (a) Radar chart showed global analysis of the representative glycan signatures in UC-EVs, EPF-EVs, and REG-EVs. (b) For individual *N*-glycan, post-hoc analysis was further executed to examine the detailed glycan difference in three methods. *P* values calculated from Fisher's least significant difference (LSD) multiple comparison test was categorized into five levels. (c) sPLS-DA score plot of *N*-glycan profiling of EVs isolated from serum of three healthy controls by UC, EPF, and REG. (d) Heatmap and hierarchical clustering analysis of 54 *N*-glycans in UC-EVs, EPF-EVs, and REG-EVs. (e) Volcano plots of differential *N*-glycans in serum vs EV. The *q*-value, representing the false discovery rate (FDR) adjusted *P*-value, was calculated using the Benjamini–Hochberg procedure to correct for multiple hypothesis testing. (f) OPLS-DA score plot of *N*-glycan profiling of serum and EV. Man: mannose; F: fucosylation; S: sialylation; FC: fold change.

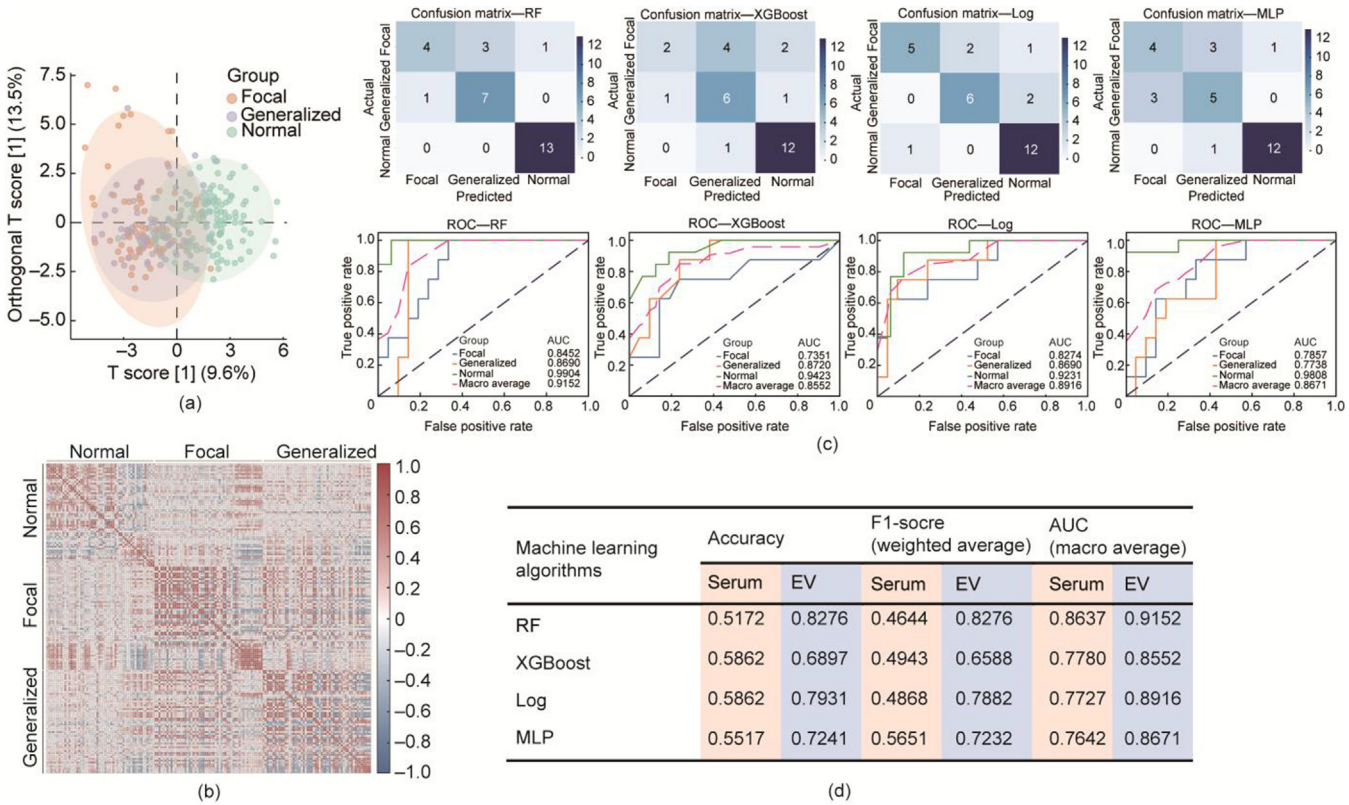

Machine learning algorithms	Accuracy		F1-socre (weighted average)		AUC (macro average)	
	Serum	EV	Serum	EV	Serum	EV
RF	0.5172	0.8276	0.4644	0.8276	0.8637	0.9152
XGBoost	0.5862	0.6897	0.4943	0.6588	0.7780	0.8552
Log	0.5862	0.7931	0.4868	0.7882	0.7727	0.8916
MLP	0.5517	0.7241	0.5651	0.7232	0.7642	0.8671

Fig. 4. *N*-glycans analysis of serum and EV from epilepsy patients. (a) OPLS-DA plot of identified *N*-glycans in EV *N*-glycan from normal, focal, and generalized patients. (b) Pearson correlation of identified EV *N*-glycans in normal, focal, and generalized patients. Bars on the right sides of the heat map show the Pearson correlation coefficient. (c) Confusion matrix and receiver operating characteristic (ROC) curve performance of the EV *N*-glycans in normal, focal, and generalized using RF, XGBoost, Log, and MLP. Metrics results of traditional machine learning methods for classification of epilepsy in serum and EV. (d) Detailed side-by-side metric comparison of biomarker between serum and EV groups. AUC: area under the curve.

distinguished normal from epilepsy groups but not between epilepsy subtypes, indicating altered glycan patterns in epilepsy with similar expression trends within the group (Fig. 4(a), Fig. S7(a) in Appendix A). These preliminary findings highlight the potential of glycans as biomarkers for childhood epilepsy.

To extend upon these observations, we performed Pearson correlation analysis on 54 sera and EV *N*-glycans across epilepsy subtypes and normal groups. Epilepsy groups demonstrated strong intra-group correlations, contrasting with weak clustering between healthy and diseased groups (Fig. 4(b), Fig. S7(b) in Appendix A). These findings indicate significant differences in glycan abundance and independent expression patterns between groups, while revealing moderate correlations between inter-subtype associations. Moreover, changes in glycan feature levels in sera and EVs further corroborated the above findings. Comparative analysis against normal controls revealed significant glycan feature alterations in epilepsy groups, particularly in bisection and sialylation. Bisected glycans (e.g., H3N5, H3N5F1, H4N5F1, H5N5) were markedly lower in abundance, while sialylated forms exhibited substantially higher numbers in both sera and EVs (Figs. S8 and S9 in Appendix A). Notably, epilepsy patients displayed elevated bisected glycans (H3N5F1, H5N5F1, and H5N5S1F1) and reduced mono-antennary H4N3S1F1 compared to controls (Fig. S10 in Appendix A). In addition, the generalized group showed decreased sialylated H6N5S1F1 and H5N5S2F1 when compared to the focal group. To understand the contribution of *N*-glycans to the variable glycan derived traits, a preliminary diagnostic evaluation of sera and EVs *N*-glycans was performed in controls and epilepsy patients. Compared with sera-derived glycans, EV glycans showed better diagnostic accuracy (Tables S4 and S5 in Appendix A). These findings align with established roles for glycosylation dynamics in neural development and synaptic function [22,30,39], strongly supporting *N*-glycans as potential epilepsy biomarkers through their disease-specific modification patterns.

To further investigate the potential of *N*-glycan signatures in diagnosing childhood epilepsy, four machine learning algorithms, random forest (RF), XGBoost, logistic regression (LR), and multilayer perceptron (MLP), were employed to analyze the test dataset. The performance of our model was evaluated using standard metrics, including accuracy, sensitivity, specificity, and F1-score.

As shown in the confusion matrix (Fig. S11(a) in Appendix A), serum *N*-glycans exhibited limited diagnostic value in making a diagnosis of epilepsy, with subpar machine learning performance across multiple algorithms. The receiver operating characteristic (ROC) curve (Fig. S11(b) in Appendix A) revealed that serum glycans achieved moderate classification accuracy, with macro-averaged area under the curve (AUC) values ranging from 0.7642 to 0.8637 for multiclass epilepsy diagnosis. In comparison, EV glycans demonstrated markedly superior diagnostic precision, as illustrated in Fig. 4(c). EV glycans yielded macro-averaged AUC values of 0.8552 to 0.9152, which significantly outperformed sera *N*-glycans. A detailed side-by-side metric comparison (Fig. 4(d)) highlights the distinct performance disparity between the two biomarker sets. This performance disparity likely stems from the ability of EV glycans to penetrate the BBB and reduced interference from highly abundant proteins present in sera samples, which lead to signal dilution in conventional serum analyses. These findings position EV-derived *N*-glycans as clinically superior biomarkers for epilepsy diagnosis and characterization.

3.5. Epilepsy diagnosis and classification via the proposed two-step machine learning model

Guided by the workflow described in Fig. 5(a) and Section S1.5 in Appendix A, we developed a two-step machine learning model for epilepsy using EV *N*-glycans. For epilepsy diagnosis (normal vs epilepsy), feature importance ranking identified candidate EV *N*-glycans (Fig. S12 in Appendix A). Recursive feature elimination was applied to this ranking, retaining the top 47 glycans as diagnostic biomarkers. For subtype classification (focal vs generalized), feature importance analysis (Fig. S13 in Appendix A) revealed that only glycans H3N4F1, H3N5F1, and H4N5 exhibited measurable importance, and these three glycans were selected as classifiers. Notably, these three subtype-specific biomarkers were members of the initial diagnostic set, strongly proposing that the complete feature collection remains consolidated at 47 biomarkers. This unified biomarker panel was used to construct epilepsy diagnosis and classification models via 4-fold cross-validation (Figs. S14 and S15 and Tables S6 and S7 in Appendix A). These models were then integrated to establish the final machine learning model for three-class epilepsy classification.

The model demonstrated robust performance on the independent test set (n = 85: normal, n = 38; focal, n = 23; generalized, n = 24): macro-averaged AUC = 0.9235 (Figs. 5(b) and (c)), accuracy = 0.8118, and F1-score = 0.8130 (Table S8 in Appendix A). In contrast, repeating this process with serum glycans yielded lower significance results: macro-averaged AUC = 0.8139 (Figs. 5(d) and (e)), accuracy = 0.6471, and F1-score = 0.6375 (Table S8), thereby reinforcing the conclusion above (Section 3.4) that EV glycans were far superior for diagnostic purposes, in comparison to serum glycans.

Furthermore, to evaluate potential effects of antiepileptic drugs (AEDs) on EV glycans, we analyzed correlations between glycan features and AED use in epilepsy patients. Among the 47 selected glycans, ten (H3N4F1, H4N4F1, H5N4S1, H5N4S1F1, H5N5S1, H5N4S2, H5N4S2F1, H5N5S2F1, H6N5S3, and H6N5S3F1) showed strong AED-associated correlations (Fig. S16 in Appendix A). Notably, four glycans (H4N4F1, H5N4S2, H6N5S3, and H3N4F1) were pivotal in constructing epilepsy diagnostic and classification models, confirming EV *N*-glycans as novel diagnostic and therapeutic targets for childhood epilepsy. These findings underscore the dynamic interplay between AEDs and glycome composition in recurrent seizures.

3.6. EV N-glycomics correlation networks for epilepsy

Monitoring dynamic changes in glycans during epilepsy can provide valuable insights into glycan characteristics closely associated with seizures. EV glycans were classified into high-mannose, complex, and hybrid types, with further subdivision into mono-, bi-, tri-, and tetra-antennary structures. Pearson correlation analysis across normal, focal, and generalized groups revealed strong intra-group correlations (e.g., within focal or generalized groups) but limited inter-group associations (off-diagonal blocks in Fig. 6(a)), indicating dynamic and partially independent glycan expression patterns in epilepsy. Subsequently, the Pearson correlation matrix was translated into a correlation network of glycans (Fig. 6(b)), where nodes represent glycans and edges denote statistically significant correlations. By applying glyco-synthetic rules [32], the biosynthetic pathways hierarchy of the 54 epilepsy-related *N*-glycans was reconstructed. As shown in the map, after the formation of a high-mannose type from a precursor, hybrid- and complex-type pathways are initiated by the addition of a GlcNAc residue to Man5GlcNAc2. Then, the hybrid-type pathway proceeds through elongation via addition of monosaccharides, while the complex-type pathway extends from Man3GlcNAc3 (Fig. 6(b)). This structured heterogeneity confirms that epilepsy-associated EV glycans adhere to conserved biosynthetic principles, linking glycan architecture to seizure-related modifications.

To fully understand glycan dynamics during progression of epilepsy, we analyzed differences in glycan correlation across focal vs normal, generalized vs normal, and generalized vs focal groups. Sialylated glycans at pathway termini exhibited upregulated trends in focal vs normal and generalized vs normal comparisons

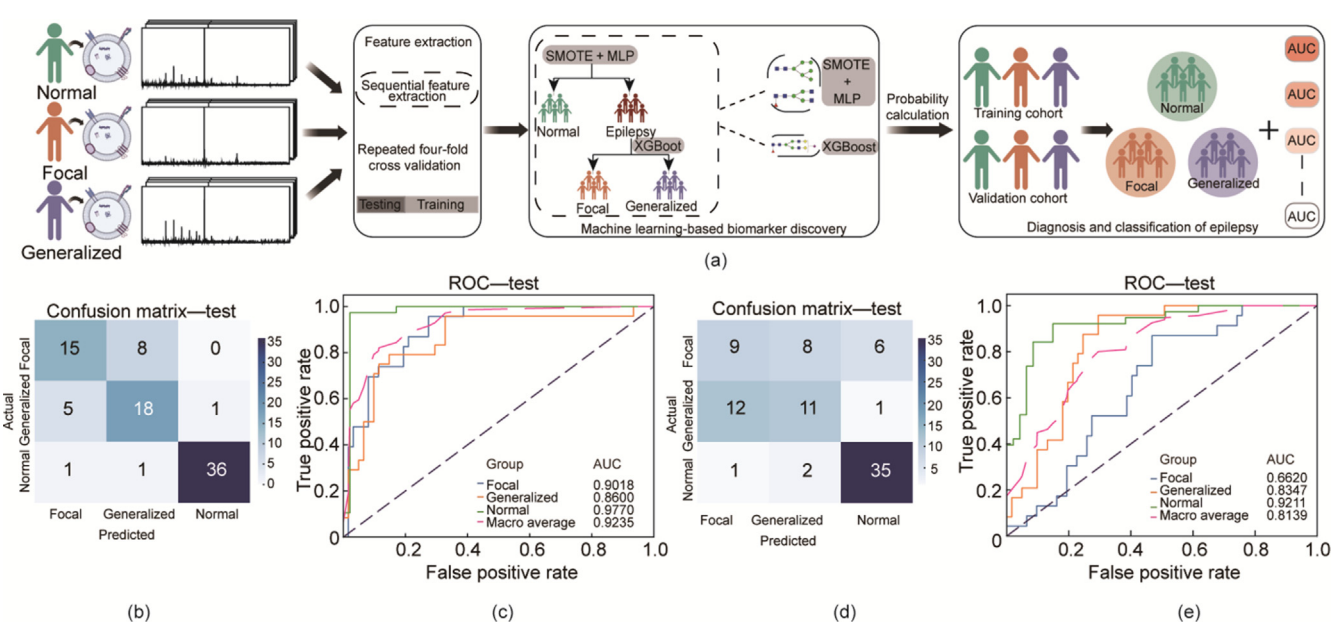

Fig. 5. Improved machine learning methods for diagnostic and classification performance in epilepsy. (a) Workflow of feature selection and machine learning model. (b) The confusion matrix represents how the improved method distinguishes between normal, focal, and generalized in the test set data based on EV *N*-glycans. (c) ROC curves represent proposed a method for normal, focal, and generalized diagnostic capabilities based on EV *N*-glycans. (d) The confusion matrix represents how the improved method distinguishes between normal, focal, and generalized in the test set data based on serum *N*-glycans. (e) ROC curves represent proposed a method for normal, focal, and generalized diagnostic capabilities based on serum *N*-glycans. SMOTE: synthetic minority oversampling technique.

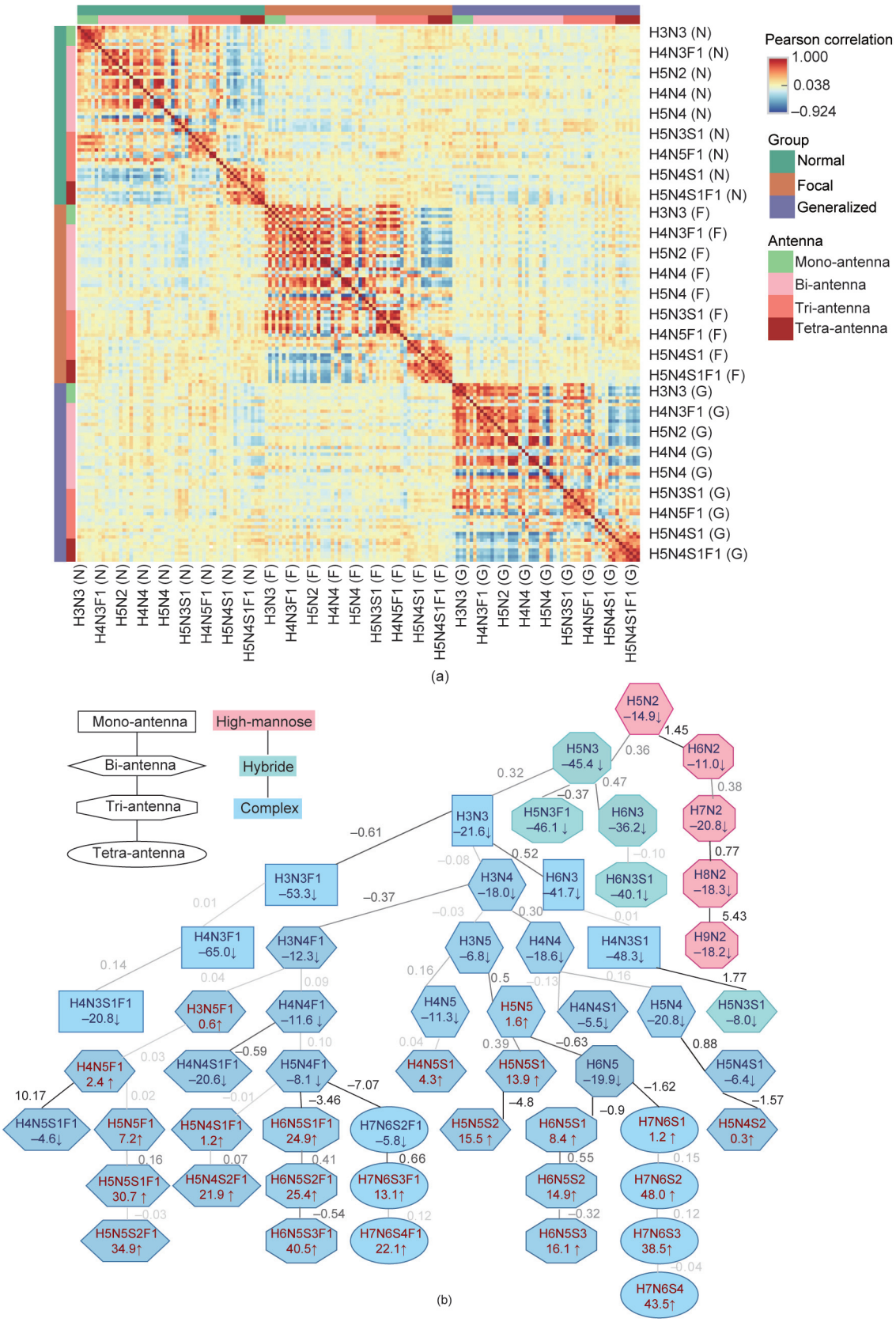

Fig. 6. Correlated changes in epilepsy EV *N*-glycans. (a) Pearson correlation characterization of differentially expressed glycan features in normal (N), focal (F), and generalized (G) groups. Three typical categories: high-mannose, complex, and hybrid, which are mono-, bi-, tri-, and tetra-antenna glycans. Partial glycans are shown in map. (b) The Pearson correlation matrix is visualized as a network. Differences between glycan correlation between focal population and normal population. Taking normal population as a reference, correlation change = correlation of connected glycan pairs in focal population-correlation of connected glycan pairs in normal population/correlation of connected glycan pairs in normal population. Red arrows represent up-regulated, blue arrows represent down-regulated. The numerical value on the line represents the degree of correlation change, and the thickness of the line represents the strength of correlation change of glycan pairs.

but were downregulated in generalized vs focal analyses (Fig. 6(b), Fig. S17 in Appendix A). Furthermore, major alterations occurred predominantly in bi-antennary complex glycans, comprising mainly of sialylation and high mannose enrichment. Specifically, key glycan pairs displayed marked correlation shifts. For example, H8N2 to H9N2, H4N4F1 to H4N4S1F1, H4N5F1 to H4N5S1F1, H5N4S1 to H5N4S2, H5N4F1 to H6N5S1F1 and H7N6S2F1, and H6N5 to H6N5S1 and H7N6S1. H4N5F1 to H4N5S1F1 correlations increased by 3.97-fold in generalized vs normal and 10.17-fold in focal vs normal, but only by 0.56-fold in generalized vs focal (Fig. S17). These changes aligned with ranking of glycan importance determined from diagnostic models, suggesting that alterations in glycan synthesis strongly contribute to childhood epilepsy pathogenesis. Overall, this systematic profiling approach elucidated molecular mechanisms underlying seizure-associated EV glycome remodeling.

4. Discussion

Glycan patterns are altered in diseases such as cancer, neurological disorders, inflammatory conditions, and immune related disorders [40]. While serum glycans show potential in cancer diagnosis, there is a need to improve their specificity [34,37,41–43]. Previous studies have shown that EVs play a critical role in transferring functional molecules (e.g., nucleic acids, lipids, proteins, and sugars) between cells, facilitating intercellular communication in both physiological and pathological environments [44]. In this process, glycans significantly influence protein function and exhibit greater stability in circulation compared to proteins and nucleic acids [45]. Despite this, most EV-based liquid biopsy studies have focused on proteins or nucleic acids, with limited attention given to EV glycans [46]. Serum-derived EVs are emerging as promising non-invasive biomarkers for neurological disorders, outperforming whole serum where limitations arise due to complexity of the serum and attenuated disease signals.

EV surface glycan patterns show high potential in efforts to identify biomarkers and pathological causes in neurological disorders [22,23,30,47]. Notably, aberrant glycan signatures on central nervous system (CNS)-derived EVs have been identified during disease progression, in particular, surface biomarkers such as L1 cell adhesion molecule, glutamate aspartate transporter, and myelin oligodendrocyte glycoprotein [48]. In Alzheimer's disease, a prevalent neurological disorder, sialylation levels and branched glycan structures are reduced while high-mannose glycans are elevated [49]. Critically, pharmacological blockade of *N*-glycan maturation using mannosidase inhibitors disrupts amyloid precursor protein (APP) transport and proteolytic processing [50]. Conversely, overexpression of sialyltransferase ST6GAL1 potentiates APP secretion and amyloid beta peptide (Aβ) production [51]. Furthermore, EVs mitigate epilepsy-related cerebral damage by regulating neuroinflammation and inhibiting post-seizure cytokine storms. Gamma-aminobutyric acid (GABA) interneuron and medial ganglionic eminence-derived EVs significantly suppress seizures [52], proposing EV glycans as novel biomarkers for non-invasive detection. However, the complexity of clinical samples and the structural diversity of glycans pose significant challenges to accurate EV glycan analysis. To overcome these challenges, we characterized EVs isolated from serum using different methods. Our findings show that EPF-EVs produced the highest EV yield and purity, with minimal protein contamination, compared to UC and REG. These results underscore the efficiency of EPF for serum EV extraction, consistent with previous studies [53], and emphasize the necessity for detailed characterization of EV populations across different isolation techniques.

EV glycosylation is a challenging yet emerging field in disease research [46]. Various methods, such as lectin-based techniques [21,54] and combined microfluidic and surface-enhanced Raman scattering techniques [55], have been developed to detect EV glycans. In this study, EV glycans isolated using different methods (UC, EPF, and REG) showed heterogeneous profiles, particularly for high mannose glycosylation, fucosylation, and sialylation. Furthermore, EPF-EVs exhibited greater glycan diversity compared to UC-EVs and REG-EVs, which closely resembled serum glycan profiles. Thus, EPF was proved to be the most effective method for isolating serum EVs, highlighting its potential for EV glycosylation biomarker discovery. Serum and EV glycan patterns share similarities but also exhibit differences as a result of biological factors (e.g., glycosyltransferase activity and EV secretion dynamics) [18] and technical factors (e.g., selective enrichment during extraction) [53,54]. We postulate that the observed similarity arises from the following aspects. Firstly, direct biogenetic linkage occurs as exosomes incorporate host cell membrane and cytosolic components (including glycoproteins) through inward budding of intracellular multivesicular bodies [46]. Serum glycoproteins may be endocytosed or adsorbed onto EVs, establishing *N*-glycan homogeneity [56]. EVs also selectively encapsulate specific glycoproteins (e.g., CD63 and CA125) released into serum, with their lipid bilayer protecting these glycoproteins from degradation and maintaining glycosylation stability [46,56]. Secondly, in terms of technical limitations during isolation, current separation methods inadequately remove serum components sharing similar physicochemical properties (e.g., size and density) with EVs [14]. Co-isolated serum glycoconjugates are detected during glycan analyses, leading to EVs exhibiting serum-like glycan profiles. Finally, molecular validation in pathological states demonstrates that 11 *N*-glycans (e.g., complex-type fucosylated/sialylated glycans) show synchronous upregulation in both serum and exosomes, with higher modification ratios in exosomes [57]. This indicates exosomes not only inherit serum glycosylation features but also undergo dynamic remodeling in the tumor microenvironment, resulting in highly correlated glycan profiles. These differences reflect distinct biosynthetic, functional, and metabolic dynamics, offering valuable insights for biomarker research. Therefore, by utilizing EPF and glycomic profiling, we characterized *N*-glycan trajectories in childhood epilepsy subtypes, demonstrating their biomarker potential through statistical and machine learning analyses.

Distinct machine learning strategies improve glycan-based diagnostics and biomarker discovery [34]. Using a proposed two-stage modeling strategy, we successfully constructed a diagnostic model by dividing the three-class classification task into two parallel binary classification tasks: epilepsy diagnosis (patients vs healthy controls) and subtype classification (focal vs generalized). Integrating these tasks yielded a hierarchical model validated on test data. We identified 47 *N*-glycan panels as potential biomarkers that demonstrated excellent performance in distinguishing focal, generalized, and normal groups. Notably, in clinical applications, EV glycan-based diagnostics outperformed serum-based methods due to the ability of EVs to cross the BBB, concentrate cell-specific cargo, and protect molecules from degradation [47]. Thus, EV glycans represent promising epilepsy biomarkers, with the identified *N*-glycan panel offering potential for the development of diagnostics and treatment strategies.

Correlation network analysis showed significant changes in complex bi-antennary glycan correlations, mainly between normal and epileptic groups, with sialylation and high mannose levels as the main changes. While focal and generalized epilepsy glycosylation profiles were normal, quantitative differences remain. These specific glycan alterations support epilepsy subtyping diagnosis via EV glycans and propose glycoengineering targets. As EV surface

glycosylation plays a critical role in cellular uptake [18], targeted glycoengineering modulation offers the dual benefits of ① optimizing the cell-type (e.g., neurons) or organ-specific targeted EV delivery efficiency and ② enabling precise targeted delivery of AEDs by regulating the uptake process, thereby providing diagnostic and therapeutic utility. These benefits support the development of glycoengineered EV glycan formulations (e.g., nasal sprays) as innovative strategies for novel AEDs, to enable more efficient, convenient, and target-specific therapies [26,58]. Furthermore, during epileptogenesis, the dynamic changes in EV glycosylation likely reflect the regulatory outcomes of specific biological processes (e.g., neuron–glia interactions) [26]. This would enable deeper exploration of glycan-mediated signal transduction functions in neurological disorders. Specifically, the following avenues can be explored: ① precise intervention in glycosylation signaling pathways using glycan-modifying enzymes to elucidate the biological functions of specific glycan structures; ② comparing glycan networks from healthy vs epileptic individuals to identify aberrant glycosyltransferase activity and reveal epilepsy-related regulatory mechanisms. Data from these studies will provide a solid foundation for the clinical translation of glycomedicine, for epilepsy towards predictive, preventive, and personalized precision medicine.

While EV glycans show promise for childhood epilepsy detection, further improvements are needed to facilitate clinical application. Additional functional validation studies on *N*-glycans are required to uncover biological mechanisms and identify intervention targets. As the cohort of epilepsy patients in this study was limited to the east Asian population in central China, a rigorously designed prospective study on a cohort with diverse geographic and ethnic representation is essential for global clinical translation. Further research is also needed to explore the feasibility of *N*-glycan fingerprinting for epilepsy diagnosis and subtype classification. Lastly, expanding the cohort size is necessary to validate the clinical utility of EV glycan profiling for diagnosis, monitoring, and prognosis.

5. Conclusion

Our study demonstrated that EPF is optimal for isolating serum EVs from large-scale clinical samples and revealing distinct EV glycosylation patterns. We comprehensively characterized differences between serum and EV-derived glycans. In a clinical study of 281 individuals, 47 *N*-glycan panels were identified as biomarkers for diagnosis and classification of childhood epilepsy using EV glycomics and a novel two-step machine learning algorithm. These biomarkers effectively distinguish normal, focal, and generalized epilepsy subtypes, outperforming serum *N*-glycans in diagnostic performance. This represents a pioneering advancement in epilepsy-related N-glycomics, with potential applications in early detection, diagnosis, subtype classification, and treatment tracking. Additionally, a glycan synthesis correlation network offers a precise depiction of protein glycosylation in epilepsy at the molecular level, providing experimental evidence to further explore the dynamic changes in glycans during progression of epilepsy. In conclusion, *N*-glycan biomarkers are promising tools for childhood epilepsy screening and disease monitoring, contributing to the advancement of personalized healthcare.

CRediT authorship contribution statement

Yuanyuan Liu: Writing – review & editing, Writing – original draft, Visualization, Methodology, Formal analysis, Data curation, Conceptualization. **Yanbin Guo:** Writing – review & editing, Writing – original draft, Visualization, Methodology, Formal analysis. **Changzhen Li:** Data curation. **Zhiwen Huang:** Visualization, Methodology, Formal analysis, Data curation. **Xiang Liu:** Data curation. **Han Xie:** Methodology. **Wenhui Wang:** Data curation. **Lili Guan:** Methodology. **Bi-Feng Liu:** Project administration, Conceptualization. **Si Liu:** Writing – review & editing, Visualization, Supervision, Project administration, Methodology, Funding acquisition, Formal analysis. **Guoping Wang:** Writing – review & editing, Supervision, Project administration, Conceptualization. **Xin Liu:** Writing – review & editing, Project administration, Funding acquisition, Conceptualization.

Declaration of competing interest

The authors declare that they have no known competing financial interests or personal relationships that could have appeared to influence the work reported in this paper.

Acknowledgments

This work was supported by the financial support from the National Key Research and Development Program of China (2022FYC3400800), the National Natural Science Foundation of China (81827901), and the Natural Science Foundation of Fujian Province (2024J01577). The authors also thank BioRender for providing some of the graphic elements used in this study. The authors would like to express their gratitude to EditSprings for the expert linguistic services provided.

Data availability statement

The data that support the findings of this study are available from the corresponding author upon reasonable request.

Appendix A. Supplementary data

Supplementary data to this article can be found online at https://doi.org/10.1016/j.eng.2025.12.009.

References

[1] Devinsky O, Vezzani A, O'Brien TJ, Jette N, Scheffer IE, De Curtis M, et al. Epilepsy. Nat Rev Dis Primers 2018;4(1):18024.
[2] Trinka E, Kwan P, Lee B, Dash A. Epilepsy in Asia: disease burden, management barriers, and challenges. Epilepsia 2019;60(S1):7–21.
[3] Klein P, Kaminski RM, Koepp M, Löscher W. New epilepsy therapies in development. Nat Rev Drug Discov 2024;23(9):682–708.
[4] Pitkänen A, Löscher W, Vezzani A, Becker AJ, Simonato M, Lukasiuk K, et al. Advances in the development of biomarkers for epilepsy. Lancet Neurol 2016;15(8):843–56.
[5] Ryvlin P, Rheims S, Hirsch LJ, Sokolov A, Jehi L. Neuromodulation in epilepsy: state-of-the-art approved therapies. Lancet Neurol 2021;20(12):1038–47.
[6] Njoku K, Pierce A, Chiasserini D, Geary B, Campbell AE, Kelsall J, et al. Detection of endometrial cancer in cervico–vaginal fluid and blood plasma: leveraging proteomics and machine learning for biomarker discovery. EBioMedicine 2024;102:105064.
[7] Welsh JA, Goberdhan DC, O'Driscoll L, Théry C, Witwer KW. MISEV2023: an updated guide to EV research and applications. J Extracell Vesicles 2024;13(2):e12416.
[8] Wang Z, Sun X, Natalia A, Tang CSL, Ang CBT, Ong CAJ, et al. Dual-selective magnetic analysis of extracellular vesicle glycans. Matter 2020;2(1):150–66.
[9] Zhao X, Liu X, Chen T, Xie H, Li S, Zhang Y, et al. Fully integrated centrifugal microfluidics for rapid exosome isolation, glycan analysis, and point-of-care diagnosis. ACS Nano 2025;19(9):8948–65.
[10] Zhang Y, Qin X, Xu Z, Liu W, Lu H, Yang Y, et al. Electric field-resistant bubble-enhanced wash-free profiling of extracellular vesicle surface markers. ACS Nano 2025;19(8):8093–107.
[11] Qin X, Xiang Y, Mao L, Yang Y, Wei B, Lu H, et al. Buoyant metal–organic framework corona-driven fast isolation and ultrasensitive profiling of circulating extracellular vesicles. ACS Nano 2024;18(22):14569–82.
[12] Xie H, Chen D, Lei M, Liu Y, Zhao X, Ren X, et al. Freeze-thaw-induced patterning of extracellular vesicles with artificial intelligence for breast cancers identifications. Small 2025;21(4):e2408871.

[13] Wang Z, Zhou X, Kong Q, He H, Sun J, Qiu W, et al. Extracellular vesicle preparation and analysis: a state-of-the-art review. Adv Sci 2024;11(30):2401069.
[14] Yang Y, Wang Y, Wei S, Zhou C, Yu J, Wang G, et al. Extracellular vesicles isolated by size-exclusion chromatography present suitability for RNomics analysis in plasma. J Transl Med 2021;19(1):104.
[15] Nieuwland R, Siljander PR. A beginner's guide to study extracellular vesicles in human blood plasma and serum. J Extracell Vesicles 2024;13(1):e12400.
[16] Wang W. Glycomedicine: the current state of the Art. Engineering 2023;26:12–5.
[17] Williams C, Royo F, Aizpurua-Olaizola O, Pazos R, Boons G, Reichardt N, et al. Glycosylation of extracellular vesicles: current knowledge, tools and clinical perspectives. J Extracell Vesicles 2018;7(1):1442985.
[18] Nishida-Aoki N, Tominaga N, Kosaka N, Ochiya T. Altered biodistribution of deglycosylated extracellular vesicles through enhanced cellular uptake. J Extracell Vesicles 2020;9(1):1713527.
[19] Martins ÁM, Ramos CC, Freitas D, Reis CA. Glycosylation of cancer extracellular vesicles: capture strategies, functional roles and potential clinical applications. Cells 2021;10(1):109.
[20] Li Y, Zhang S, Liu C, Deng J, Tian F, Feng Q, et al. Thermophoretic glycan profiling of extracellular vesicles for triple-negative breast cancer management. Nat Commun 2024;15(1):2292.
[21] Zhang G, Huang X, Gong Y, Ding Y, Wang H, Zhang H, et al. Fingerprint profiling of glycans on extracellular vesicles via lectin-induced aggregation strategy for precise cancer diagnostics. J Am Chem Soc 2024;146(42):29053–63.
[22] Costa J, Gatermann M, Nimtz M, Kandzia S, Glatzel M, Conradt HS. N-glycosylation of extracellular vesicles from HEK-293 and glioma cell lines. Anal Chem 2018;90(13):7871–9.
[23] Dusoswa SA, Horrevorts SK, Ambrosini M, Kalay H, Paauw NJ, Nieuwland R, et al. Glycan modification of glioblastoma-derived extracellular vesicles enhances receptor-mediated targeting of dendritic cells. J Extracell Vesicles 2019;8(1):1648995.
[24] Catterall WA. Sodium channels, inherited epilepsy, and antiepileptic drugs. Annu Rev Pharmacol Toxicol 2014;54(1):317–38.
[25] Zamponi GW, Lory P, Perez-Reyes E. Role of voltage-gated calcium channels in epilepsy. Pflugers Arch 2010;460(2):395–403.
[26] Karttunen J, Heiskanen M, Lipponen A, Poulsen D, Pitkänen A. Extracellular vesicles as diagnostics and therapeutics for structural epilepsies. Int J Mol Sci 2019;20(6):1259.
[27] Gratpain V, Mwema A, Labrak Y, Muccioli GG, Van Pesch V, Des RA. Extracellular vesicles for the treatment of central nervous system diseases. Adv Drug Deliv Rev 2021;174:535–52.
[28] Conroy LR, Hawkinson TR, Young LEA, Gentry MS, Sun RC. Emerging roles of *N*-linked glycosylation in brain physiology and disorders. Trends Endocrinol Metab 2021;32(12):980–93.
[29] Bronisz E, Cudna A, Wierzbicka A, Kurkowska-Jastrzębska I. Blood–brain barrier-associated proteins are elevated in serum of epilepsy patients. Cells 2023;12(3):368.
[30] Berenguer J, Lagerweij T, Zhao XW, Dusoswa S, van der Stoop P, Westerman B, et al. Glycosylated extracellular vesicles released by glioblastoma cells are decorated by CCL18 allowing for cellular uptake via chemokine receptor CCR8. J Extracell Vesicles 2018;7(1):1446660.
[31] Liu X, Shen L, Wan M, Xie H, Wang Z. Peripheral extracellular vesicles in neurodegeneration: pathogenic influencers and therapeutic vehicles. J Nanobiotechnology 2024;22(1):170.
[32] Benedetti E, Pučić-Baković M, Keser T, Wahl A, Hassinen A, Yang JY, et al. Network inference from glycoproteomics data reveals new reactions in the IgG glycosylation pathway. Nat Commun 2017;8(1):1483.
[33] Zhai C, Xie F, Xu J, Yang Y, Zheng W, Hu H, et al. Correlation between membrane proteins and sizes of extracellular vesicles and particles: a potential signature for cancer diagnosis. J Extracell Vesicles 2023;12(12):12391.
[34] Zhang H, Liu S, Wang Y, Huang H, Sun L, Yuan Y, et al. Deep learning enhanced the diagnostic merit of serum glycome for multiple cancers. iScience 2024;27(1):108715.
[35] Wang D, Madunić K, Zhang T, Lageveen-Kammeijer GSM, Wuhrer M. Profound diversity of the N-glycome from microdissected regions of colorectal cancer, stroma, and normal colon mucosa. Engineering 2023;26:32–43.
[36] Ruhaak LR, Kim K, Stroble C, Taylor SL, Hong Q, Miyamoto S, et al. Protein-specific differential glycosylation of immunoglobulins in serum of ovarian cancer patients. J Proteome Res 2016;15(3):1002–10.
[37] Liu S, Liu Y, Lin J, Liu BF, He Z, Wu X, et al. Novel insight into the etiology of haff disease by mapping the N-glycome with orthogonal mass spectrometry. Engineering 2023;26:63–73.
[38] Shi M, Sheng L, Stewart T, Zabetian CP, Zhang J. New windows into the brain: central nervous system-derived extracellular vesicles in blood. Prog Neurobiol 2019;175:96–106.
[39] Klarić TS, Gudelj I, Santpere G, Novokmet M, Vučković F, Ma S, et al. Human-specific features and developmental dynamics of the brain N-glycome. Sci Adv 2023;9(49):eadg2615.
[40] He M, Zhou X, Wang X. Glycosylation: mechanisms, biological functions and clinical implications. Signal Transduct Target Ther 2024;9(1):1–33.
[41] Liu J, Liu S, Huang Z, Fu Y, Fei J, Liu X, et al. Associations between the serum levels of PFOS/PFOA and IgG N-glycosylation in adult or children. Environ Pollut 2020;265:114285.
[42] Liu S, Tu C, Zhang H, Huang H, Liu Y, Wang Y, et al. Noninvasive serum *N*-glycans associated with ovarian cancer diagnosis and precancerous lesion prediction. J Ovarian Res 2024;17(1):26.
[43] Wang Y, Liu S, Li J, Yin T, Liu Y, Wang Q, et al. Comprehensive serum *N*-glycan profiling identifies a biomarker panel for early diagnosis of non-small-cell lung cancer. Proteomics 2023;23(20):2300140.
[44] Yu D, Li Y, Wang M, Gu J, Xu W, Cai H, et al. Exosomes as a new frontier of cancer liquid biopsy. Mol Cancer 2022;21(1):56.
[45] Yan Y, Li R, Chen H, Li Y, Wu M, Wang Z, et al. Magnetic nanoagent assisted deciphering of heterogeneous glycans in extracellular vesicles of varied cellular origins. Biosens Bioelectron 2023;241:115705.
[46] Vrablova V, Kosutova N, Blsakova A, Bertokova A, Kasak P, Bertok T, et al. Glycosylation in extracellular vesicles: isolation, characterization, composition, analysis and clinical applications. Biotechnol Adv 2023;67:108196.
[47] del C Bravo-Miana R, Arizaga-Echebarria JK, Otaegui D. Central nervous system-derived extracellular vesicles: the next generation of neural circulating biomarkers? Transl Neurodegener 2024;13(1):32.
[48] Xu M, Zhou M, Li S, Zhen X, Yang S. Glycoproteins as diagnostic and prognostic biomarkers for neurodegenerative diseases: a glycoproteomic approach. J Neurosci Res 2021;99(5):1308–24.
[49] Zhang Q, Ma C, Chin LS, Pan S, Li L. Human brain glycoform coregulation network and glycan modification alterations in Alzheimer's disease. Sci Adv 2024;10(14):eadk6911.
[50] McFarlane I, Georgopoulou N, Coughlan CM, Gillian AM, Breen KC. The role of the protein glycosylation state in the control of cellular transport of the amyloid β precursor protein. Neuroscience 1999;90(1):15–25.
[51] Nakagawa K, Kitazume S, Oka R, Maruyama K, Saido TC, Sato Y, et al. Sialylation enhances the secretion of neurotoxic amyloid-β peptides. J Neurochem 2006;96(4):924–33.
[52] Putthanbut N, Lee JY, Borlongan CV. Extracellular vesicle therapy in neurological disorders. J Biomed Sci 2024;31(1):85.
[53] Freitas D, Balmaña M, Poças J, Campos D, Osório H, Konstantinidi A, et al. Different isolation approaches lead to diverse glycosylated extracellular vesicle populations. J Extracell Vesicles 2019;8(1):1621131.
[54] Shimoda A, Miura R, Tateno H, Seo N, Shiku H, Sawada S, et al. Assessment of surface glycan diversity on extracellular vesicles by lectin microarray and glycoengineering strategies for drug delivery applications. Small Methods 2022;6(2):2100785.
[55] Zhou Q, Niu X, Zhang Z, O'Byrne K, Kulasinghe A, Fielding D, et al. Glycan profiling in small extracellular vesicles with a SERS microfluidic biosensor identifies early malignant development in lung cancer. Adv Sci 2024;11(33):2401818.
[56] Théry C, Amigorena S, Raposo G, Clayton A. Isolation and characterization of exosomes from cell culture supernatants and biological fluids. Curr Protoc Cell Biol 2006;Chapter 3. Unit 3.22.
[57] Lv J, Wang Z, Li F, Zhang Y, Lu H. Reverse capture for selectively and sensitively revealing the N-glycome of serum exosomes. Chem Commun 2019;55(95):14339–42.
[58] Upadhya D, Shetty AK. Promise of extracellular vesicles for diagnosis and treatment of epilepsy. Epilepsy Behav 2021;121:106499.